Silica exposed-core microstructured optical fibers

Roman Kostecki,[1,*] Heike Ebendorff-Heidepriem,[1] Claire Davis,[2] Grant McAdam,[2] Stephen C. Warren-Smith,[1] and Tanya M. Monro[1]

[1] *Centre of Expertise in Photonics, Institute for Photonics & Advanced Sensing, School of Chemistry & Physics, University of Adelaide, Adelaide, SA 5005, Australia*
[2] *Defence Science and Technology Organisation, Fishermans Bend, Victoria, Australia*
[*] *roman.kostecki@adelaide.edu.au*

Abstract: We report the fabrication of silica microstructured optical fibers with the core exposed along the whole length, and characterize the stability of these new fibers when exposed to some typical sensing and storage environments. We show the fiber loss to be the best achieved to date for exposed-core fibers, while the deterioration in the transmission properties is up to ∼2 orders of magnitude better than for the previously reported exposed-core fibers produced in soft glass. This opens up new opportunities for optical fiber sensors requiring long term and/or harsh environmental applications while providing real time analysis anywhere along the fibers length.

OCIS codes: (060.2280) Fiber design and fabrication; (060.2290) Fiber materials; (060.2310) Fiber optics; (060.2370) Fiber optics sensors; (060.4005) Microstructured fibers; (160.6030) Silica; (300.1030) Absorption.

References and links

1. P. Kasier, E. A. J. Marcatili, and S. E. Miller, "A new optical fiber," Bell Sys. Tech. J. **52**, 265–269 (1973).
2. J. C. Knight, T. A. Birks, P. S. J. Russell, and D. M. Atkin, "All-silica single-mode optical fiber with photonic crystal cladding," Opt. Lett. **21**, 1547–1549 (1996).
3. T. M. Monro, W. Belardi, K. Furusawa, J. C. Baggett, N. G. R. Broderick, and D. J. Richardson, "Sensing with microstructured optical fibres," Meas. Sci. Technol. **12**, 854–858 (2001).
4. T. Monro, D. Richardson, and P. Bennett, "Developing holey fibres for evanescent field devices," Electron. Lett. **35**, 1188–1189 (1999).
5. O. S. Wolfbeis, "Fiber-optic chemical sensors and biosensors," Anal. Chem. **80**, 4269–4283 (2008).
6. T. M. Monro and H. Ebendorff-Heidepriem, "Progress in microstructured optical fibers," Annu. Rev. Mater. Res. **36**, 467–495 (2006).
7. J. Lægsgaard and A. Bjarklev, "Microstructured optical fibers—fundamentals and applications." J. Am. Ceram. Soc. **89**, 2–12 (2006).
8. T. M. Monro, S. Warren-Smith, E. P. Schartner, A. François, S. Heng, H. Ebendorff-Heidepriem, and S. Afshar V., "Sensing with suspended-core optical fibers," Opt. Fiber Technol. **16**, 343–356 (2010).
9. H. Ebendorff-Heidepriem, S. C. Warren-Smith, and T. M. Monro, "Suspended nanowires: fabrication, design and characterization of fibers with nanoscale cores," Opt. Express **17**, 2646–2657 (2009).
10. L. Tong, R. R. Gattass, J. B. Ashcom, S. He, J. Lou, M. Shen, I. Maxwell, and E. Mazur, "Subwavelength-diameter silica wires for low-loss optical wave guiding," Nature **426**, 816–819 (2003).
11. K. Kiang, K. Frampton, T. Monro, R. Moore, J. Tucknott, D. Hewak, D. Richardson, and H. Rutt, "Extruded singlemode non-silica glass holey optical fibres," Electron. Lett. **38**, 546–547 (2002).
12. H. Ebendorff-Heidepriem, P. Petropoulos, S. Asimakis, V. Finazzi, R. Moore, K. Frampton, F. Koizumi, D. Richardson, and T. Monro, "Bismuth glass holey fibers with high nonlinearity," Opt. Express **12**, 5082–5087 (2004).

#173379 - $15.00 USD Received 30 Jul 2012; revised 21 Sep 2012; accepted 22 Sep 2012; published 2 Oct 2012

13. J. Leong, P. Petropoulos, J. Price, H. Ebendorff-Heidepriem, S. Asimakis, R. Moore, K. Frampton, V. Finazzi, X. Feng, T. Monro, and D. Richardson, "High-nonlinearity dispersion-shifted lead-silicate holey fibers for efficient 1-μm pumped supercontinuum generation," J. Lightwave Technol. **24**, 183–190 (2006).
14. J. Jensen, P. Hoiby, G. Emiliyanov, O. Bang, L. Pedersen, and A. Bjarklev, "Selective detection of antibodies in microstructured polymer optical fibers," Opt. Express **13**, 5883–5889 (2005).
15. A. S. Webb, F. Poletti, D. J. Richardson, and J. K. Sahu, "Suspended-core holey fiber for evanescent-field sensing," Opt. Eng. **46**, 010503 (2007).
16. T. G. Euser, J. S. Y. Chen, M. Scharrer, P. S. J. Russell, N. J. Farrer, and P. J. Sadler, "Quantitative broadband chemical sensing in air-suspended solid-core fibers," J. Appl. Phys. **103**, 103108 (2008).
17. A. Mazhorova, A. Markov, A. Ng, R. Chinnappan, O. Skorobogata, M. Zourob, and M. Skorobogatiy, "Label-free bacteria detection using evanescent mode of a suspended core terahertz fiber," Opt. Express **20**, 5344–5355 (2012).
18. S. Afshar V., S. C. Warren-Smith, and T. M. Monro, "Enhancement of fluorescence-based sensing using microstructured optical fibres," Opt. Express **15**, 17891–17901 (2007).
19. E. P. Schartner, H. Ebendorff-Heidepriem, S. C. Warren-Smith, R. T. White, and T. M. Monro, "Driving down the detection limit in microstructured fiber-based chemical dip sensors," Sensors **11**, 2961–2971 (2011).
20. Y. Ruan, E. P. Schartner, H. Ebendorff-Heidepriem, P. Hoffmann, and T. M. Monro, "Detection of quantum-dot labelled proteins using soft glass microstructured optical fibers," Opt. Express **15**, 17819–17826 (2007).
21. H. Yan, J. Liu, C. Yang, G. Jin, C. Gu, and L. Hou, "Novel index-guided photonic crystal fiber surface-enhanced Raman scattering probe," Opt. Express **16**, 8300–8305 (2008).
22. A. Bjarklev, J. B. Jensen, J. Riishede, J. Broeng, J. Laegsgaard, T. T. Larsen, T. Sorensen, K. Hougaard, and O. Bang, "Photonic crystal structures in sensing technology," Proc. SPIE **5502**, 9–16 (2004).
23. J. E. Debs, H. Ebendorff-Heidepriem, J. S. Quinton, and T. M. Monro, "A fundamental study into the surface functionalization of soft glass microstructured optical fibers via silane coupling agents," J. Lightwave Technol. **27**, 576–582 (2009).
24. Y. L. Hoo, W. Jin, C. Shi, H. L. Ho, D. N. Wang, and S. C. Ruan, "Design and modeling of a photonic crystal fiber gas sensor," Appl. Opt. **42**, 3509–3515 (2003).
25. C. M. B. Cordeiro, C. J. S. de Matos, E. M. dos Santos, A. Bozolan, J. S. K. Ong, T. Facincani, G. Chesini, A. R. Vaz, and C. H. B. Cruz, "Towards practical liquid and gas sensing with photonic crystal fibres: side access to the fibre microstructure and single-mode liquid-core fibre," Meas. Sci. Technol. **18**, 3075–3081 (2007).
26. C. Martelli, P. Olivero, J. Canning, N. Groothoff, B. Gibson, and S. Huntington, "Micromachining structured optical fibers using focused ion beam milling," Opt. Lett. **32**, 1575–1577 (2007).
27. A. van Brakel, C. Grivas, M. N. Petrovich, and D. J. Richardson, "Micro-channels machined in microstructured optical fibers by femtosecond laser," Opt. Express **15**, 8731–8736 (2007).
28. J. P. Parry, B. C. Griffiths, N. Gayraud, E. D. McNaghten, A. M. Parkes, W. N. MacPherson, and D. P. Hand, "Towards practical gas sensing with micro-structured fibres," Meas. Sci. Technol. **20**, 075301 (2009).
29. F. M. Cox, R. Lwin, M. C. J. Large, and C. M. B. Cordeiro, "Opening up optical fibres," Opt. Express **15**, 11843–11848 (2007).
30. S. C. Warren-Smith, H. Ebendorff-Heidepriem, T. C. Foo, R. Moore, C. Davis, and T. M. Monro, "Exposed-core microstructured optical fibers for real-time fluorescence sensing," Opt. Express **17**, 18533–18542 (2009).
31. S. Warren-Smith, E. Sinchenko, P. Stoddart, and T. Monro, "Distributed fluorescence sensing using exposed core microstructured optical fiber," IEEE Photon. Technol. Lett. **22**, 1385–1387 (2010).
32. K. Peters, "Polymer optical fiber sensors—a review," Smart Mater. Struct. **20**, 013002 (2011).
33. H. Ebendorff-Heidepriem, K. Kuan, M. R. Oermann, K. Knight, and T. M. Monro, "Extruded tellurite glass and fibers with low OH content for mid-infrared applications," Opt. Mater. Express **2**, 432–442 (2012).
34. H. Ebendorff-Heidepriem and T. M. Monro, "Extrusion of complex preforms for microstructured optical fibers," Opt. Express **15**, 15086–15092 (2007).
35. S. C. Warren-Smith, H. Ebendorff-Heidepriem, S. Afshar V., G. McAdam, C. Davis, and T. Monro, "Corrosion sensing of aluminium alloys using exposed-core microstructured optical fibres," Mater. Forum **33**, 110–121 (2009).
36. K. Richardson, D. Krol, and K. Hirao, "Glasses for photonic applications," Int. J. Appl. Glass Sci. **1**, 74–86 (2010).
37. M. Li and D. Nolan, "Optical transmission fiber design evolution," J. Lightwave Technol. **26**, 1079–1092 (2008).
38. Heraeus Quarzglas GmbH & Co. KG, *Pure Silica Rods for Specialty Fiber Applications*, 1st ed. (2012), http://heraeus-quarzglas.com/.
39. D. Wildeboer, F. Jeganathan, R. G. Price, and R. A. Abuknesha, "Characterization of bacterial proteases with a panel of fluorescent peptide substrates," Anal. Biochem. **384**, 321–328 (2009).
40. M. Y. Sim and S. Gleixner, "Studying the etch rates and selectivity of SiO_2 and Al in BHF solutions," in *2006 16th Biennial University/Government/Industry Microelectronics Symposium* (2006), pp. 225–228.
41. C. J. Voyce, A. D. Fitt, and T. M. Monro, "Mathematical modeling as an accurate predictive tool in capillary and microstructured fiber manufacture: the effects of preform rotation," J. Lightwave Technol. **26**, 791–798 (2008).
42. M. Fujiwara, K. Toubaru and S. Takeuchi, "Optical transmittance degradation in tapered fibers," Opt. Express

#173379 - $15.00 USD Received 30 Jul 2012; revised 21 Sep 2012; accepted 22 Sep 2012; published 2 Oct 2012

19, 8596–8601 (2011).
43. D. Tallant, T. Michalske, and W. Smith, "The effects of tensile stress on the Raman spectrum of silica glass," J. Non-Cryst. Solids **106**, 380–383 (1988).
44. G. Brambilla, F. Xu, and X. Feng, "Fabrication of optical fibre nanowires and their optical and mechanical characterisation," Electron. Lett. **42**, 517–519 (2006).
45. G. Zhai and L. Tong, "Roughness-induced radiation losses in optical micro or nanofibers," Opt. Express **15**, 13805–13816 (2007).
46. R. Brandsch, G. Bar, and M.-H. Whangbo, "On the factors affecting the contrast of height and phase images in tapping mode atomic force microscopy," Langmuir **13**, 6349–6353 (1997).

1. Introduction

Microstructured optical fibers [1] (MOFs) are well-suited for sensing, as characteristic longitudinal air holes used to provide the effective refractive index needed for light confinement [2] can also act as tiny sample chambers [3]. The portion of guided light located within these holes can be used to provide the light-matter overlap needed for many fiber optic sensing applications [4, 5]. Unlike conventional optical fibers, MOFs can be manufactured from a single material [6], and with the appropriate cross-sectional design, the structure can provide the broad range of optical properties demanded by sensors [7].

For MOFs, the portion of guided light (often described as "*evanescent field*") protruding into the holes of the structure is affected by the characteristics of the medium within these holes [4]. This light-matter overlap provides opportunities for exploiting the interaction of light with gases and liquids, where the absorption and fluorescence characteristics can be used to determine the composition and concentration of the analyte [5]. In this regard, the fiber geometry can provide extremely long interaction lengths without the need for large volumes. Of particular interest is the suspended-core fiber [8], which can have a significant fraction of the guided power located within the holes [9], since the geometry has a high air filling fraction with a small core suspended on a number of thin struts. Unlike glass nano-wires [10], this design provides a means for obtaining uniform micrometer-nanometer scale suspended 'wires' while protecting the highly sensitive core, and long lengths can be fabricated by drawing a structured preform.

The suspended-core fiber has been demonstrated in soft glasses [11–13], polymer [14] and silica [15] materials. Chemical [15, 16] and biological [17] suspended-core fiber absorption spectroscopy sensors, which exploit the absorbance characteristics of the light-matter overlap, provide opportunities for both environmental sensing and quantitative chemical analysis. Suspended-core fiber sensors using in-fiber excitation and recapturing [18] of fluorescent dyes [19] or quantum dots [20], as well as surface-enhanced Raman spectroscopy using nanoparticles [21], have also been shown to provide highly sensitive specificity of the analyte of interest.

In principle, the suspended-core fiber also offers the potential for easier filling compared to MOFs with hexagonally arranged cladding holes that provide a small air filling fraction when the core is small [22]. In practice, the time needed to fill suspended-core fibers depends on the required interaction length and size of the holes, such as $\sim$7 hrs for gas diffusion [15] or $\sim$100 min for water at standard temperature and pressure [23], along a 1 m length of fiber with Ø8 μm holes. This makes their use impossible for real time or distributed sensing applications and difficulty still exists when attempting to ensure stable optical coupling while filling. To overcome these problems, fabrication techniques which expose the core [24] have been demonstrated by micro-machining fluidic side-channels at several locations along the fiber length [25–28], which results in short exposed regions in the order of tens of microns. This provides access to the core by the analyte, making it useful for real time sensing applications. However, in applications where kinetic changes of the analyte need to be measured, where emp-

#173379 - $15.00 USD Received 30 Jul 2012; revised 21 Sep 2012; accepted 22 Sep 2012; published 2 Oct 2012

tying and re-filling is required, or long lengths are needed for distributed sensing applications, post processing methods to the fiber still remain impractical. Another technique to expose the core is by creating an opening at the preform stage of fiber fabrication. This provides a means to fabricate long lengths of exposed-core fiber, and has been demonstrated in polymer [29] (polymethylmethacrylate) and soft glass [30] (Schott F2) materials, where the geometry was shown to be practical for real time evanescent field and distributed sensing [31] applications, with the capacity for fast filling and quick response to kinetic changes of the analyte.

Both polymer and soft glasses have properties which makes them useful for particular applications [9, 32, 33], and their glass transition temperatures (T_g) are low enough to make them practical for extruding the structured preform [34]. Nevertheless, these materials are not transparent at UV wavelengths, where many biological molecules can absorb the light, and the soft glass exposed-core fiber deteriorated quickly [30, 35], making it impractical for long term and/or harsh environmental applications. On the other hand, silica is known to be reliable under a range of processing and use environments, with relatively better mechanical and thermal stability [36]. Highly homogeneous, high purity bulk material is commercially available, which has led to silica telecom fibers regularly being made with low loss ($\sim$0.2 dB/km at NIR wavelengths) [37]. Also, silica has a relatively low refractive index, which can improve the sensitivity of evanescent field sensors, since reducing the index contrast (Δn) at the core-cladding boundary increases the power fraction to the analyte or functionalized surface [19].

In this paper we demonstrate an alternative fabrication technique for glass exposed-core fibers, where the fabricated geometry is a useful platform for surface analysis of the core. We report, for the first time to the best of our knowledge, the fabrication of a silica microstructured fiber with the core exposed along the whole length, and characterize the stability of this new fiber when exposed to some typical sensing and storage environments.

2. Silica exposed-core fiber fabrication

2.1. Introduction to silica exposed-core fiber fabrication

The aim of this work was to develop silica exposed-core fibers (Fig. 1), which are asymmetric and therefore needed new fabrication methods to be established. These methods expand on a combination of work previously shown by Webb *et al.* [15] for fabricating silica suspended-core fibers (wagon wheel structure) by machining the preform, and Warren-Smith *et al.* [30] for cutting a thin slot into the side of the symmetric preform (soft glass) in order to expose the core region. High purity fused silica known as Suprasil F300HQ (Heraeus Quarzglas GmbH & Co.KG) was chosen because it is produced to be free from bubbles and made to tight geometric tolerances [38]. This material has high transmission in the UV-Vis-NIR spectral range making it suitable for (bio)chemical sensing applications since it allows for the efficient excitation of a range of fluorophores; for example quantum dot labeled proteins excited in the visible [20] and fluorogenic peptide substrates excited in the UV [39].

2.2. The preform

The exposed-core fiber preform was fabricated from Ø12 mm F300HQ silica rod, which was drilled with three holes, where the centers of the holes form an equilateral triangle. The preform was sonic cleaned in methanol and Milli-Q water, then etched for 30 minutes in a buffered hydrofluoric acid solution (BHF), made using 6 volumes of ammonium fluoride (NH_4F, 40% solution) to 1 volume of hydrofluoric acid (HF, 50% solution), which has a well known etch rate of 100–250 nm/min [40]. After etching, the preform was rinsed with de-ionized water and then sonic cleaned in methanol and Milli-Q water, after which it was dried with nitrogen. The only difference between suspended-core fiber and exposed-core fiber preforms, is that for the exposed-core fiber case a slot was cut along the length of one of the holes, as shown in Fig. 1(a).

#173379 - $15.00 USD Received 30 Jul 2012; revised 21 Sep 2012; accepted 22 Sep 2012; published 2 Oct 2012

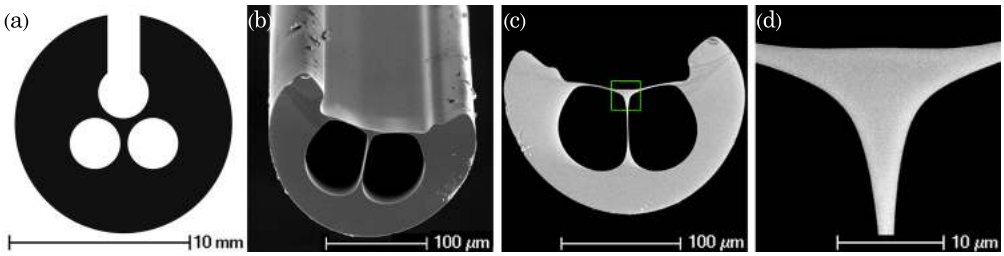

Fig. 1. (a) Cross section of the preform fabricated from Ø12 mm F300HQ silica rod; and, scanning electron microscope images of (b) the silica exposed-core fiber with (c) the cross section measured at the maximum to be Ø202 μm; and, (d) an enlarged image of the core having an effective diameter of 10.0μm.

2.3. Fiber drawing

To draw the preform to fiber a 6m tower with graphite resistance furnace, positive pressurization system and automated diameter control was used. By systematically using a series of temperatures and pressures, hole expansion and draw characteristics were investigated for the process of producing suspended-core fibers using the preform described in the previous section. These investigations showed that the exposed-core fiber could be produced using a temperature of 2000°C with pressure at 1.4 kPa, although one should consider that temperature and pressure profiles can vary between drawing towers and furnace designs [41].

A single 127 m long uncoated exposed-core fiber (Fig. 1(b)) was fabricated and the dimensions of this fiber were measured using cross-sectional images from a scanning electron microscope (SEM), shown in Figs. 1(b)–1(d), being Ø202 μm (measured at the maximum) with each hole being Ø66.0 μm, defined as the diameter of a circle whose area is equal to the cross sectional area of the hole. The central web thickness (between the holes) is 0.85 μm minimum, while the webs each side of the core are 1.10 μm minimum thickness. The core, shown by the green box in Fig. 1(c) and enlarged in Fig. 1(d), has an effective diameter of 10.0 μm, defined as the diameter of a circle whose area is equal to a triangle that fits wholly within the core area [9].

3. Silica exposed-core fiber characterization

3.1. Fiber loss & fluorescence

After fabrication, the exposed-core fiber was stored in the laboratory, exposed to air, on a high density Polyurethane foam drum with 1 m circumference. While the fiber was on the drum, cutback fiber loss measurements were performed by coupling the light from a 100 W halogen light bulb source with power curve of approximately Gaussian distribution and peak power at 800 nm, into one end of the exposed-core fiber. At the other end, the light from the core was imaged onto the grating of a Ando AQ6315E Optical Spectrum Analyzer (OSA) such that the power was maximized before each measurement. The fiber loss measurement results taken directly after fiber draw, shown by the red spectrum in Fig. 2(a), were 1.12 ± 0.15 dB/m, 1.10 ± 0.08 dB/m and 1.43 ± 0.39 dB/m at 532 nm, 900 nm and 1550 nm respectively. Further work is required to determine the cause of the increased loss at longer wavelengths. For another fiber loss measurement taken 26 days after fiber draw, shown by the blue spectrum in Fig. 2(a), the results were observed to be the same within a 95% confidence interval. As a comparison, the fiber loss measurement results for a suspended-core fiber produced in the same way, with material from the same bulk stock, and with similar core, web and hole sizes as for the exposed-core fiber, is shown by the black spectrum in Fig. 2(a). This suspended-core fiber result, being

#173379 - $15.00 USD Received 30 Jul 2012; revised 21 Sep 2012; accepted 22 Sep 2012; published 2 Oct 2012

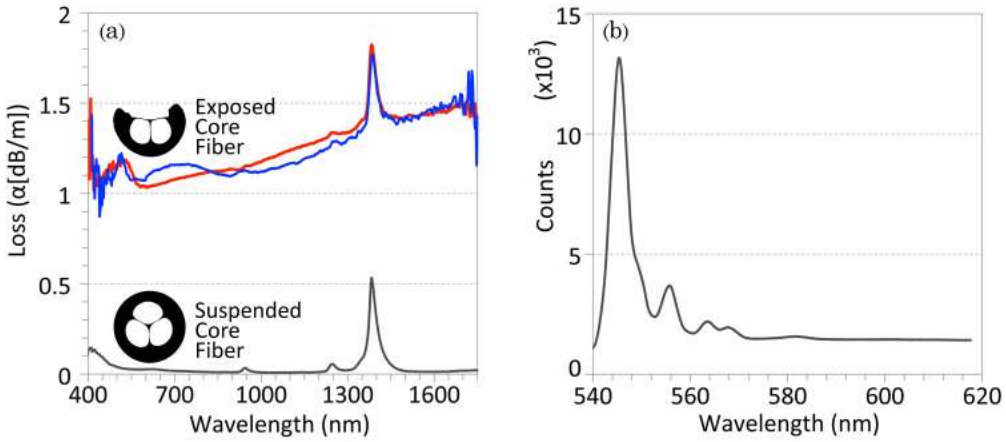

Fig. 2. (a) Loss of silica exposed-core fiber, broadband cutback measurements taken 26 days apart (red and blue) compared to silica suspended-core fiber with similar core size (black); and, (b) fiber Raman peaks at 532 nm.

$\sim$2 orders of magnitude lower compared to the exposed-core fiber, shows that confinement loss is negligible in the total loss of the exposed-core fiber, and therefore additional surface scattering loss, either from the process of cutting the slot or airborne particulates depositing on the surface of the core [42] before or after fiber drawing, is the most likely cause of the additional loss. For exposed-core fibers previously produced in Schott F2 lead silicate soft glass [30] ($n \sim$1.62) with a core size of $\sim$ Ø3 µm, the fiber loss measurements taken directly after fiber draw were 5.54$\pm$0.20 dB/m, 2.25$\pm$0.26 dB/m and 2.50$\pm$0.34 dB/m at 532 nm, 900 nm and 1550 nm respectively. Further work is required to determine the effect that core size has on the fiber loss of the silica exposed-core fiber.

Another factor which can restrict the detection limit of a fiber optic sensor is the amount of Raman and fluorescence peaks generated within the glass [19] which depends on the wavelength and power of the light source. Given enough power and with a sensitive enough detector, the Raman spectrum corresponding to the energy of the probed vibrational modes of the silica is expected, whereas fluorescence is an indication of impurities and/or structural defects within the silica material. In order to detect the Raman and any potential fluorescence peaks, a 25 mW laser excitation light source at commonly used 532 nm was coupled into a 1 m long exposed-core fiber using a 60$\times$ objective via a dichroic mirror. The signal collected from the fiber was imaged using the same objective, passed through the dichroic mirror and filtered using a 532 nm long pass filter, and measured using a Horiba iHR550 Imaging Spectrometer with Synapse CCD Detector. The peaks observed at 545 nm, 550 nm, 555 nm, 562 nm, 566 nm and 580 nm, shown in Fig. 2(b), correspond to well known Raman peaks of silica at 490 cm^{-1}, 605 cm^{-1}, 800 cm^{-1}, 1050 cm^{-1}, 1190 cm^{-1} and 1600 cm^{-1} respectively, previously used for sensing applications [43]. The absence of any fluorescence peaks shows that the silica material has negligible fluorescence at 532 nm for the excitation power and detector sensitivity used. For fluorescence or Raman spectroscopy sensing applications these peaks generated within the glass might affect the detection limit, depending on the excitation and emission wavelengths of interest.

#173379 - $15.00 USD Received 30 Jul 2012; revised 21 Sep 2012; accepted 22 Sep 2012; published 2 Oct 2012

3.2. *Environmental stability*

3.2.1. Introduction to environmental stability

Numerous sensing applications in health, the environment, agriculture and national security involve the detection of analyte typically suspended in a bulk liquid or gas; such as water or air. When preparing the fiber for these applications, solvents such as acetone, isopropanol, methanol and water are sometimes also used [44] to clean the core of dust or other particulates deposited on the surface. The silica exposed-core fiber serves as a unique platform for measuring any deterioration in the transmission properties when exposed to these typical sensing and processing environments, providing access to the core for post exposure surface analysis.

In previous studies, for the exposed-core fibers produced in F2 soft glass [30, 35] with a $\sim$ Ø3 µm core, it was found that the fiber loss increased by $0.4\pm0.048\,\mathrm{dBm^{-1}day^{-1}}$, even when stored in a dry nitrogen filled environment. It is thought that this deterioration in the transmission properties of the fiber occurs due to changes in the properties at the core surface, such as particulate deposits [42], micro-fracturing [44] and/or increased roughness [45] induced by exposure to the environment. Since the deterioration found in the F2 soft glass exposed-core fibers was rapid, it could easily be measured by comparing standard cutback loss measurements over time. However, as shown in the previous section no loss was observed after 26 days for the silica exposed-core fiber.

3.2.2. Exposure to air, water & methanol

To measure the exposure induced deterioration in the transmission properties of the silica exposed-core fiber, a length of fiber was setup as previously described for cutback loss measurements. Instead of performing cutbacks, the transmitted power spectrum, in dBm, was recorded from 350–1750 nm every two minutes. With the fiber in air, this setup was left long enough so that the measured power stabilized to within ±0.05 dBm, then used to take time based measures of the power. Then any changes over time in the transmission characteristics can be fitted to the equation,

$$P_{\lambda,t} = P_{\lambda,0}10^{-\xi t/10} \tag{1}$$

where ξ is the loss in dB/day. An assumption for these measurements is that the deterioration measured comes from changes along the exposed fiber length, not just the cleaved ends of the fiber, as the area exposed along the length is much greater than the area at the ends. As a sanity check, a laboratory-grade patch cord optical fiber assembly was setup in the same way, to ensure that the measured losses were not coming from the light source or other parts of the setup; where no deterioration was detected.

The result of ξ_λ (Eq. (1)) for a 4.2m length of the exposed-core fiber exposed to air for 180hrs is shown in Fig. 3(a), where the 95% confidence interval is also shown in black. This result shows that there is a sharp loss peak at 515 nm, equivalent to $0.043\,\mathrm{dBm^{-1}day^{-1}}$, and a broad loss from $\sim$450 nm to $\sim$900 nm with a peak of $0.023\,\mathrm{dBm^{-1}day^{-1}}$. At wavelengths $\sim$900 nm to $\sim$1340 nm the loss is at $\sim0.0043\,\mathrm{dBm^{-1}day^{-1}}$, and drops below the detection limit of the experiment for wavelengths $>\sim$1340 nm. The air exposure induced deterioration in the transmission properties of the silica exposed-core fiber is lower than the confidence intervals for cutback measurements, as shown in Fig. 2(a), and $\sim$2 orders of magnitude better than for the previously reported exposed-core fibers produced in F2 soft glass.

This measurement was repeated for a 1m length of the silica exposed-core fiber with a 8cm centrally located section of the fiber submersed in Milli-Q water, shown in Fig. 3(b), where we observe that the transmission properties of the fiber is reduced by $\sim0.067\,\mathrm{dBm^{-1}day^{-1}}$ for wavelengths shorter than 1450 nm. When this was repeated with methanol, it was observed that the transmission properties of the silica exposed-core fiber was significantly affected across all

#173379 - $15.00 USD Received 30 Jul 2012; revised 21 Sep 2012; accepted 22 Sep 2012; published 2 Oct 2012

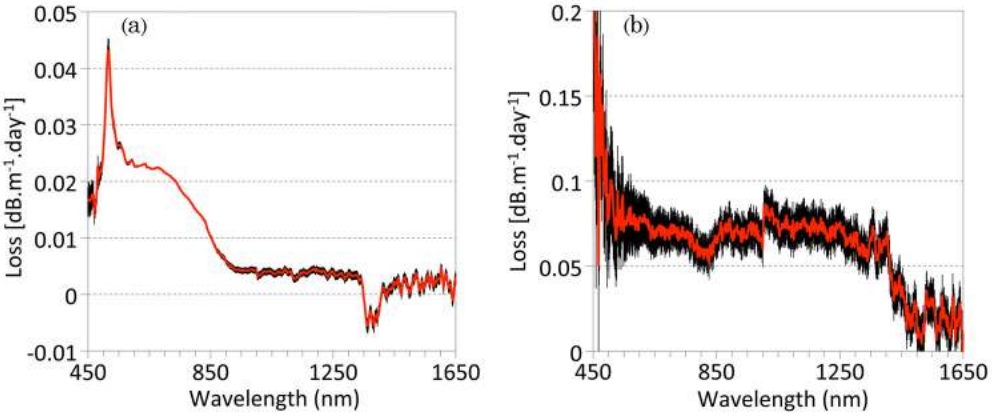

Fig. 3. Deterioration in the transmission properties of the silica exposed-core fiber when exposed to (a) air; and, (b) water.

the measured wavelengths (350–1750 nm), at a rate of 12.8–16.8 $\mathrm{dBm^{-1}hr^{-1}}$.

This deterioration in the transmission properties is expected to come from changes in the mechanical and/or compositional characteristics at the core surface, causing light scattering effects. When the core diameter is reduced, these light scattering effects are expected to increase, as a greater portion of guided light travels outside the core. Further work is required to quantitatively determine the effect that core size has on the deterioration in the transmission properties of the silica exposed-core fiber.

3.2.3. Surface mechanical and compositional characteristics

In order to determine the differences between the mechanical and compositional characteristics of the exposed sample surfaces, nanometer-scale topographical and phase mapping of the exposed-core fiber core surfaces was performed using a NT-MDT Ntegra Solaris AFM with Smena head for Tapping Mode Atomic Force Microscopy (AFM).

Figures 4(a)–4(c), 4(d)–4(f) and 4(g)–4(i) show the AFM phase and topology results of a 25 μm^2 section across the core for the exposed-core fiber exposed to air for 19 days, Milli-Q water for 72 hrs and methanol for 2 hrs respectively. For the core area exposed to air, the nanometer scale spikes in the topology and phase shift suggest small hardened impurities within the surface structure, while the bulk of the material is homogeneous in composition with nanometer scale roughness. For the core exposed to water, large peaks measuring > 100 nm in height and several microns across the surface suggest that impurities from the water have been deposited onto the core. The darkest areas in the phase image show up on the topology to be slightly lower than the surrounding bulk, which may also be an indication of surface damage such as micro-fracturing [44]. The results for the core exposed to methanol shows micron scale areas with large phase shifts where the topology image indicates a increase in height. The methanol exposed-core area was further investigated using a ContourGT-K1 coherence scanning interferometer (CSI), shown in Fig. 4(j), which indicates micrometer scale pitted sections along the core instead of the increase in height observed by the AFM. It is known that topology height reversal can occur for AFM images when the tip is strongly affected by the capillary forces and also by the tip-sample van der Waals attraction [46]. In this interaction regime, the phase shift shows to be more negative on more hydrophilic regions, and suggests pitting or micro-fracturing of the methanol exposed sample, which is confirmed by the CSI results. Nevertheless, further experimental evidence would be needed to confirm these hypothesis.

#173379 - $15.00 USD Received 30 Jul 2012; revised 21 Sep 2012; accepted 22 Sep 2012; published 2 Oct 2012

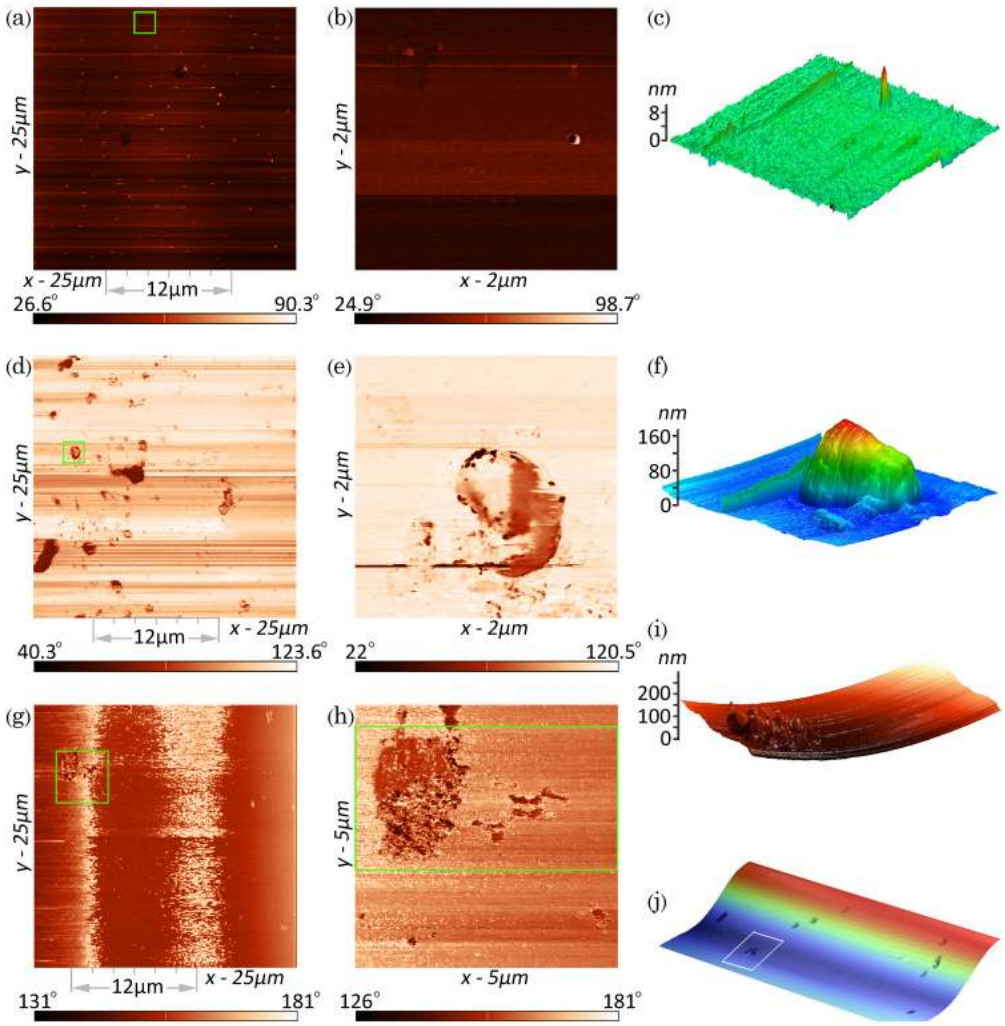

Fig. 4. Tapping Mode Atomic Force Microscopy images of the exposed-core fibers exposed to (a)–(c) air, (d)–(f) water and (g)–(i) methanol with (j) a coherence scanning interferometer image along the methanol exposed core region. (a), (d) and (g) show the phase images across the core region indicated by the 12 µm area on the *x*-axis, with [(b), (e) and (h) respectively] enlarged phase images of the area shown by the green box; and, (c), (f) and (i) showing their respective topologies.

4. Conclusion

A silica exposed-core fiber has been fabricated, for the first time to the best of our knowledge. We have demonstrated preform drilling as an alternative for fabricating glass exposed-core fibers, and shown the unique ability to perform surface analysis of the core with the silica exposed-core fiber geometry produced. We explored and characterized the new silica exposed-core fiber, showing it to have relatively low loss with deterioration in the transmission properties being $\sim$2 orders of magnitude better than for the previously reported exposed-core fibers produced in soft glass. Although the silica material shows good stability in air and water, the buildup of contaminates on the surface and micro-fracturing deteriorates the transmission prop-

#173379 - $15.00 USD Received 30 Jul 2012; revised 21 Sep 2012; accepted 22 Sep 2012; published 2 Oct 2012

erties, while significant degradation occurs with the use of methanol.

With high transmission properties in the UV-Vis-NIR spectral range, the silica material is suitable for (bio)chemical sensing applications. The exposed-core geometry serves as a versatile platform for real time evanescent field absorption or fluorescence spectroscopy, with capacity for fast filling and quick response to kinetic changes of the analyte. This opens up new opportunities for optical fiber sensors requiring long term and/or harsh environmental applications while providing long length light interaction with the analyte of interest.

In the future, further practical issues need to be solved, particularly in how to package the fiber such that it is sensitive to the chosen analyte but protected from the applied sensing environment.

Acknowledgments

The authors acknowledge Peter Henry for his contribution to the silica fiber drawing. T. Monro acknowledges the support of an Australian Research Council Federation Fellowship.

#173379 - $15.00 USD Received 30 Jul 2012; revised 21 Sep 2012; accepted 22 Sep 2012; published 2 Oct 2012